Available online at www.sciencedirect.com
SCIENCE DIRECT
Biochimica et Biophysica Acta 1763 (2006) 345–355
BIOCHIMICA ET BIOPHYSICA ACTA
BBA
http://www.elsevier.com/locate/bba

Systematic search for the rate constants that control the exocytotic process from chromaffin cells by a Genetic Algorithm

Aviv Mezer [a], Uri Ashery [c], Menachem Gutman [a,*], Elad Project [a], Eran Bosis [a], Gadi Fibich [b], Esther Nachliel [a]

[a] *Laser Laboratory for Fast Reactions in Biology, Department of Biochemistry, Tel Aviv University, Israel*
[b] *Department of Applied Mathematics, Tel Aviv University, Israel*
[c] *Department of Neurobiochemistry, Tel Aviv University, Israel*

Received 22 September 2005; received in revised form 9 February 2006; accepted 10 February 2006
Available online 27 March 2006

Abstract

We have recently created a kinetic model that reproduces the dynamics of exocytosis with high accuracy. The reconstruction necessitated a search, in a multi-dimensional parameter space, for 37 parameters that described the system, with no assurance that the parameters, which reconstructed the observations, are a unique set. In the present study, a Genetic Algorithm (GA) was used for a thorough search in the unknown parameter space, using a strategy of gradual increase of the complexity of the analyzed input data. Upon systematic incorporation of one to four measurable parameters, used as input signals for the analysis, the constraint set on the GA search imposed the convergence of the free parameters into a single narrow range. The mean values for each adjustable parameter represent a minimum for the fitness function in the multi-dimensional parameter space. The GA search demonstrates that the parameters that control the kinetics of exocytosis are the rate constants of the steps downstream to synaptotagmin binding, and that the equilibrium constant of the binding of calcium to Munc13 controls the calcium-dependent priming process. Thus, the systematic use of the GA creates a link between specific reactions in the process of exocytosis and experimental phenotypes.

Keywords: Genetic Algorithm (GA); Exocytosis; Rate constant; Kinetic analysis; Chromaffin cell; Synaptic protein

1. Introduction

Communication between neurons is carried out by a synchronous exocytosis of synaptic vesicles. The exocytotic process is mediated by a sequence of interactions between cytosolic, vesicular and plasma membrane proteins. In the last decades, the roles of specific proteins involved in this process have been intensively studied [1–7]. However, the exact sequence of events that leads to exocytosis is still not fully understood. Chromaffin cells have been extensively used to study the involvement of synaptic proteins in vesicle exocytosis using high time resolution membrane capacitance measurements [5]. These measurements provided valuable information about the kinetics of exocytosis and the effect of proteins on different kinetic components of secretion.

Recently, we presented an innovative mathematical analysis based on a kinetic model [8] that links up the partial reactions between the participating proteins into a comprehensive mechanism that describes exocytosis. The model is based on a description of the interactions between the proteins involved in the exocytotic process, using a set of well-defined first and second order rate equations (Scheme 1). When these equations are propagated in time, the solution reconstructs the experimental measurements with all their fine details. Moreover, the model can also reproduce the outcome of complex experimental protocols and the effect of genetic manipulations of specific proteins.

The model reconstruction necessitated a search, in a multi-dimensional parameter space, for 37 parameters that described the system. However, there was no assurance that the

* Corresponding author. Tel.: +972 3 6409824; fax: +972 3 6409875.
E-mail address: me@hemi.tau.ac.il (M. Gutman).

0167-4889/$ - see front matter © 2006 Elsevier B.V. All rights reserved.
doi:10.1016/j.bbamcr.2006.02.011

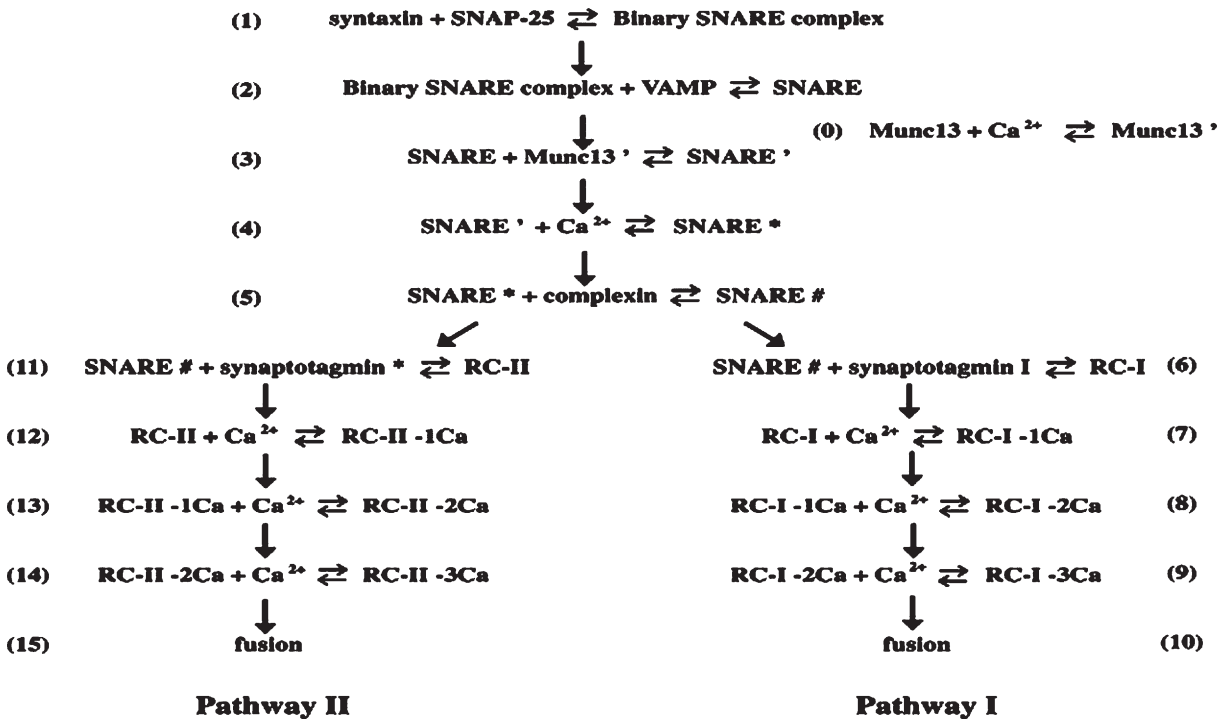

Scheme 1. The sequence of events used in the model to simulate the exocytotic process as published at Mezer et al. [8].

parameters, which reconstruct the observation, were a unique set. However, the inherent complexity of the system renders it very sensitive to the value of the parameters. Accordingly, the values of all parameters must be simultaneously determined. This calls for a systematic search over a multi-dimensional parameter space for any combination of constants that satisfactorily reconstruct the observed signal. Only when the solution is unique and represents a global minimum of the fitness function in the parameter space (see Methods), the magnitude of the rate constants could be physically interpretable. In the present publication, we achieved this goal by applying the Genetic Algorithm (GA) for the evaluation of the uniqueness of the rate constants determined for a complex set of reactions of the exocytosis model.

Since its first presentation by Holland [9], the GA attracted much interest and was applied to a multitude of scientific fields, including molecular modeling, polymer design, protein folding etc. (for review [10] and references therein). Yet, its application to the analysis of complex biochemical processes was rather limited, and only a few attempts were made to utilize the GA for solving chemical kinetic problems [11–15]. Recently, we had applied the GA to an automated search for the rate constants of a large, multi-equilibria system and demonstrated that the analysis of the results can indicate whether the solution is indeed the unique global minimum in the parameter space [16]. In that study, we discovered that fitting a single observation is not sufficiently restrictive; the search could yield a large number of combinations of parameters, each of them being an acceptable reconstruction of the signal. On the other hand, when increasing the number of the analyzed signals, the system becomes more restrictive and the solution converges into the global minimum.

The present publication demonstrates that the exocytosis process is reconstructed by a unique set of parameters. The analysis was applied to fit measurements that were collected under various experimental protocols, each of which emphasized a different phase of the maturation-fusion process. Under these conditions, where the optimization follows the different aspects of the process, the GA consistently converged to a single set of values, suggesting it is, the global minimum of the fitness function in the multi-dimensional parameter space. The set of parameters that was found through the GA was shown to reproduce the lag time of the release reaction, a feature which was not optimized for. Moreover, we show that a gradual increase in the complexity of the analyzed signals restricted the range of parameters and indicated the reactions that control specific aspects of exocytosis.

2. Methods

2.1. The model system

The process of exocytosis is presented as a linear array of interactions between synaptic proteins (Scheme 1, adjusted from Mezer et al. [8]). Each step consists of a reaction between well-defined reactants and is characterized by forward and backward rate constants. The ratio between the off rate constants (k_{-i}) and the on rate constants (k_i) is equal to the equilibrium constant (K_i). The reaction mechanism is basically linear, where the product of one step is the reactant of the next one. A detailed description of the model can be found in Mezer et al. [8]. Briefly, the modeling of the exocytotic process was imitated with the formation of reaction between SNAP25 and syntaxin I to form the binary SNARE complex [17–19]. This complex reacts with the third SNARE protein, the synaptobrevin/VAMP II, to form the mature ternary SNARE complex [17,20,21]. The process moves forward by sequential activations steps; at first, by the active form of munc13-1 (marked as munc13′), and then by the reaction of calcium ions with a high affinity site to form the intermediate

Table 1
The published parameters used in the calculations

Constant	Present analysis *	Reference
$k_1 = \sim 6 \times 10^3$ M^{-1} s^{-1}	>500 M^{-1} s^{-1}	[44]
$K_1 = \sim 126$ nM	≤100 nM	[19]
$k_{-2} = \sim 42 \times 10^{-5}$ s^{-1}	<0.01 s^{-1}	[45]
$k_2 > 1 \times 10^5$ M^{-1} s^{-1}	>1×10^4 M^{-1} s^{-1}	[8]
$k_5 = \sim 3 \times -10^7$ M^{-1} s^{-1}		[24]
$k_{-5} = \sim 0.38$ s^{-1}		
[SNAP25]: excess	>0.1 μM	[18,46]
[Syntaxin]: excess	>0.1 μM	

The rate and equilibrium constants are numbered as in Scheme 1.
* According to the present analysis the magnitude of the adjustable parameter must be larger than the indicated value.

SNARE*. The next step in the maturation is the binding of complexin to the SNARE* to form the SNARE$^{\#}$ complex [22–25]. At this intermediate stage, there is a bifurcation of the main pathway into two competing reactions. One pathway (Path I) represents the reaction of Synaptotagmin1 (SytI) with the mature SNARE-complexin adducts, to form the first releasable complex (RC-I), which can participate in a rapid fusion process. The second pathway (Path II), emerging also from the same SNARE-complexin adduct, is due to reaction with an alternate Ca^{2+} sensor, Synaptotagmin* (Syt*) to form the second population of releasable complex (RC-II), which fuses significantly slower. When the intracellular Ca^{2+}-concentration increases, each of the two paths reacts successively with three calcium ions and the vesicles fuse with the cell membrane [26–29]. Besides the mainstream process, we had to add a parallel one-step event (reaction 0) representing a Ca^{2+} dependant activation step. The novel Ca^{2+} activated step could have been assigned also to unknown, hypothetical reactants. Yet, to simplify the system we attributed this function to a defined protein, Munc13-1. Munc13-1 was shown to be a priming factor in neurons and has three C2 calcium-binding domains and one calmodulin binding site [30–32]. Accordingly and in order to avoid addition of unknown reactants, step 0 was defined as activation of Munc13-1 (It should be stated that, provided that the activation step can be mediated either by free Ca^{2+} or through reaction with calmodulin, the overall mechanism is still the same in both cases).

The experimental protocol, simulated in this study, is the flash-photolysis of caged Ca^{2+} [33,34]. In this protocol, the chromaffin cells are dialyzed with solution containing a permeable caged Ca^{2+} compound, under conditions where the free Ca^{2+} concentration is maintained at a constant level (usually 200–300 nM Ca^{2+}, but the level can be adjusted during the experiment). After 2 min of equilibration (the pre-pulse step), a flash of UV light elevates the [Ca^{2+}] to 10–50 μM for 5 s (flash stimulation) and secretion is measured continuously by a membrane capacitance measurement.

The simulation program reconstructed the same protocol as previously described [8]. Briefly, the reactions between all proteins were propagated for a period of 10 min. at 50 nM Ca^{2+}, representing the situation inside the cells before the pre-pulse step. The final concentrations of the intermediates were used at the end of this period as the initial concentrations for the pre-pulse step, which was set as 2-min simulation in the presence of 280 nM [Ca^{2+}]. The concentrations of the intermediates, as calculated at the end of the pre-pulse, were used as the initial values for the final simulation of the pulse, where the [Ca^{2+}] concentration was set to 30 μM.

2.2. Range of variance set for the adjustable parameters

The rate and equilibrium constants were allowed to vary from the upper limit set by the Debye–Smoluchowski equation [35], down to a few orders of magnitude below (for more details, see Mezer et al. [8]). Rate and equilibrium constants that had been published were used in the model without any change and are summarized in Table 1. The concentration of the vesicles was set to 10 nM [8].

The reconstruction of the signals is attained by a search in a multidimensional parameter space. The definition of the adjustable parameters, their upper and lower limits and the final values derived by the analysis, are all listed in Table 2.

2.3. The fitting problem

To gain high confidence in the results of the analysis, the fitness function was initially calculated for a pair of experimental result input curves: the exocytosis from wild type (WT) cells and from synaptotagminI KO (SytIKO) cells.

For any given set of values of the unknown parameters, the ordinary differential equations can be solved using standard numerical sub-routines such as Matlab's ODE23s. The level of agreement between the experimental signals and the numerical solutions can be expressed by a fitness function (Ft), which is weighed as an average of the squares of the differences between the calculated

Table 2
The adjustable parameters used for the reconstruction of the exocytotic dynamics in chromaffin cells

Reaction	Variable	Search range	Result range	Mean	Standard deviation
0) munc13′ + Ca^{2+} → munc13	k_0	1E4–1E9	9E5–7E8	1.52 E8	1.81 E8
	K_0	10E-9–1000E-9	265E-9–602E-9	451 E-9	126 E-9
	[munc13]	1E-10–1E-8	1.3E-10–1E-9	4.36 E-10	2.51 E-10
3) SNARE + munc13′ → SNARE′	k_3	1E5–1E8	4.3E7–6.4E7	2.03 E7	1.25 E7
	K_3	1E-10–1E-6	1.5E-8–7.3E-7	1.3 E-7	2.13 E-7
4) SNARE′ + Ca^{2+} → SNARE*	k_4	1E4–1E9	1.4E6–2E7	0.843 E7	0.638 E7
	K_4	10E-9–1000E-9	16.5E-9–468E-9	224 E-9	192 E-9
5) SNARE* + complexin → SNARE#	[complexin]	10 E-8–100e-8	100E-9–640E-9	335 E-9	188 E-9
6) SNARE# + synaptotagmin1 → RC-I	k_6	1E5–1E8	2.9E7–1.44E8	5.71 E7	3.7 E7
	K_6	1E-10–1E-7	2.6E-9–7.9E-9	4.27 E-9	1.75 E-9
7–9) RC-I + Ca^2 → RC-I-Ca	k_9	1E4–10E8	2.7E6–6.5E6	4.73 E6	1.25 E6
	k_{-9}	3–3000	29.5–160	92.5	47.5
10) RC-I-3Ca → fusion	k_{10}	3–30,000	1150–2996	2630	690
11) SNARE# + synaptotagmin* → RC-II	k_{11}	1E5–1E8	1.7E7–9.1E7	4.55 E7	2.51 E7
	K_{11}	1E-10–1E–7	3E-9–9E-9	5.68 E-9	1.87 E-9
12–14) RC-II + Ca^2 → RC-I I-Ca	k_{14}	1E4–10E8	2.4E6–7E6	4.91 E6	1.40 E6
	k_{-14}	3–30,000	55–230	145	64.5
15) RC-II-3Ca → fusion	k_{15}	3–30,000	5.7–99	22.5	28.5

The table lists the reactions that were included in the model (for details, see Scheme 1), the nature of the variable (concentration, rate constant or equilibrium constant), the range at which the parameter was allowed to vary, the range reached by the search (using all penalty factors), the means of the best 10 results and their standard deviation.

solutions ($X_t^{\text{calculated}}$) and the measured signals (X_t^{signal}) and is normalized with respect to the calculated signal.

$$ft(t) = \sum_t \left(\frac{(\text{calculated WT}_t - \text{signal WT}_t)}{\text{signal WT}} \right)^2 + \left(\frac{(\text{calculated KO}_t - \text{signal KO}_t)}{\text{signal WT}} \right)^2 \quad (1)$$

This basic expression is the sum of two fitting functions; one corresponds to the dynamics measured for the WT (wild type), while the other is for the SytIKO mutant. To account for the fact that most exocytosis occurs during the first second after stimulation, the fitness function values that were calculated for the first second (t=0 till t=1 s) were multiplied by 2 (weighed with a factor of 2). This correction factor is referred to as P_6 in Appendix A.

Further improvement of the fitting procedure was gained by addition of others experimental features as an input for the reconstruction. Thus, when the search was also set to optimize the dependence of the exocytotic burst amplitude on the pre-pulse Ca^{2+} concentration, the values of the fitness function, as calculated by Eq. (1), were adjusted according to the procedure detailed in Appendix A. In brief, the program calculated the release dynamics for the 'WT' case at varying pre-pulse [Ca^{2+}] and related the amplitude calculated at [Ca^{2+}]=180 and 1640 nM with that of 540 nM. These ratios (r(1) and r(2), respectively) were converted into penalties P_1 and P_2 as detailed in Appendix A.

The fourth constraint was the addition of the kinetics constraint of the recovery of exocytosis following exhaustive stimulation. The algorithm mimicked the exhaustion phase of the cell by a 8 μM Ca^{2+} pulse for 400 ms, followed by a recovery phase (Δt) that varied in length from 0 to 100 s. At the end of the recovery time, the [Ca^{2+}] was set to 30 μM, and the amplitudes of RC-I and RC-II at t=1 s were calculated. The ratios of the amplitudes at the time points 0s; 10 s and 100 s were compared, and the appropriate penalty factors (P_3, P_4 and P_5) were calculated (see Appendix A).

To determine the uniqueness of the solution, the analysis was repeated many times, and those combinations of parameters that yielded a fitness function value of less than Ft=300 were subjected to statistical quantile analysis. In the case where the values assigned by the program for each adjustable parameter appear as a linear function, the values of the adjustable parameter are considered to be members of a normal population, and the mean value corresponds to the minimum of the fitness function along the given axis of the multidimensional parameter space. The combination of all means represents the global minimum of the fitness function.

2.4. Genetic algorithm

In cases of high-dimensional optimization problems with possible non-smooth fitness function and multiple local minima, the optimization of the fitness function can be performed by the application of the GA. In the present study, each generation consisted of 100 "genotypes", each of them having a random set of adjustable parameters that were selected within the permitted range (see Table 2). The program used these values to reconstruct several experimental signals, and to calculate the fitness. At the end of the generation, the best-fit phenotype was cloned and replaced the worst fitting one. Apart from that, the genes were manipulated by the following alternations: two heuristicX-over, two arithXover, two simpleXover, four boundaryMutation, five multi-NonUnifMutation, ten nonUnifMutation and two unifMutation. All these genetic manipulations are standard procedures and defined in the GAOT program of Matlab [13]. The fitness function was calculated for all new combinations and their values were evaluated, both among the present generation and with respect to those genotypes of the previous generation.

Our choice of Matlab as the computational platform is motivated by its portability across different platforms and by the availability of the GA toolbox GAOT [13]. To demonstrate the robustness of our methodology, we used the default parameters of GAOT, rather than trying to optimize performance by varying GAOT's parameters (the selection and termination functions, etc.).

In the present study, the GA searched for the minimum of the fitness function in an 18–12 dimensional space. The length of a 3000–6000 generations' run required duration from 10 to 24 h, depending on the processor in use.

3. Results and discussion

3.1. Application of the genetic algorithm on standard input signals

In order to test whether the GA is capable of searching over the parameter space and achieving a satisfactory result within a reasonable time (~24 h), we used the set of differential rate equations and parameters that were determined by Mezer et. al. [8] to generate a pair of simulated input curves. The first input curve corresponds to the dynamics of exocytosis as measured from control chromaffin cells, while the second input curve corresponds with the dynamics of exocytosis recorded from chromaffin cells derived from synaptotagmin I knockout mice (SytIKO) [36]. The two curves that perfectly fit the experimental data [8]) were then reconstructed by the GA. The analysis by the algorithm was repeated 10 times, and each time for 6000 generations. In all cases, the fitting was improved and after ~1000 generations, the program reconstructed the input signals with high accuracy, retracing them almost within the width of the line (Fig. 1a).

The evolution of the fitting process can be presented either by the convergence of the fitness function (Fig. 1b), or by the variance of the adjustable parameters as a function of the

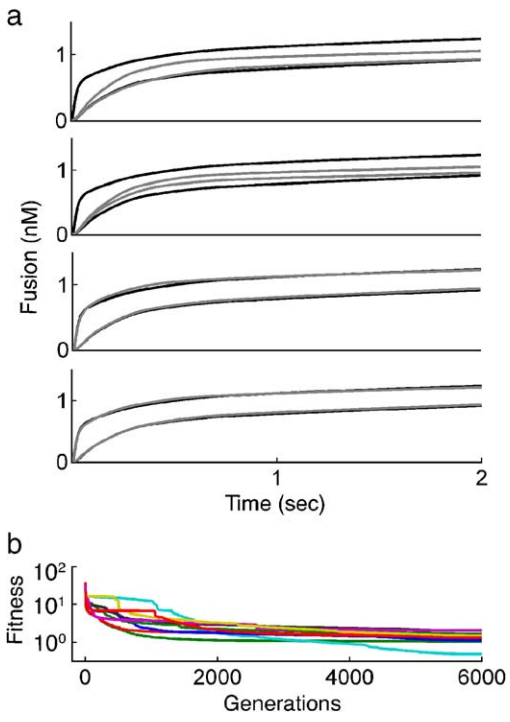

Fig. 1. (a) The best-fit phenotype with the progression of the GA evolution. The upper frame represents the reconstructed lines (gray curves), together with the input curves describing the experimental signals for WT (upper black curve) and SytIKO (lower black curve), as calculated for the first generation. The lower frames represent the enhanced fitting as recorded after 4, 10 and 6000 generations, respectively. It should be noted that the reconstructed curve after 6000 generations practically overlaps the experimental input curves. (b) The convergence of the fitness function of the input signals during repeated simulations as a function of the generation number. The value of the fitness function is defined in Eq. (1). Color represents different runs.

number of generations (Fig. 2). As seen in Fig. 1b, the values of the fitness function decreased during the evolution, as the number of generation increased by 2–3 orders of magnitude. When the value of the fitness function is less than ~3, the input signal and its reconstruction practically overlap. However, the evolution of the improvement of the fitness function as a function of the number of generations varied significantly among the different runs (Fig. 1b). In some cases, the fitness function declined monotonically, while in other cases, the decrease was stepwise. This is an indication that the search was random each time but converged to the same, low fitness (Fig. 1b). Further examination of later stages of the graphs describing the fitness function suggested that extension of the process beyond 3000 generations is not necessary, since the fitness function did not improve significantly behind 3000 generations. Thus, throughout this study, the simulations were terminated after 3000 generations, reducing the calculation time by ~50%.

In contrast to the significant improvement of the GA fitness over the generation as suggested by the fitness function, some of the parameters that were selected by the GA significantly diverged. In some cases, the convergence of the parameters was acceptable (for example, the range of k_9 and k_{15} converged to one order of magnitude; Fig. 2a and b). But, during the very same runs, other parameters hardly converged at all (for example, see the divergence of K_6 and K_0 in Fig. 2c, and d which varied 3–4 orders of magnitude). Thus, although the quality of the reconstructions was very satisfactory, each of the runs reached a different local minimum in the multi-dimensional parameter space. The widespread range of the values indicated that, even if the reconstruction appeared to be successful, we did not reach a global minimum and there are several sets of parameters that can equally reconstruct these curves. Nevertheless, a successful convergence of a certain parameter implies that it is crucial for the reconstruction of the observation and that it controls the kinetics of the fitted system.

We next examined whether the same set of parameters converged while fitting to the experimental curves. We obtained a similar convergence (not shown) for the artificial input curves (Fig. 1 and Fig. 2). Interestingly, the parameters that converged by the GA are the K_d's of the synaptotagmin binding (reactions 6 and 11), the 3 parallel low affinity calcium binding steps (reactions 7–9, 12–14) and the last steps of fusion (reactions 10 and 15). On the basis of the successful reconstruction of the experimental fusion dynamics, we concluded that these parameters control the kinetics of exocytosis from wt and SytIKO cells. The values that we obtained are similar to the

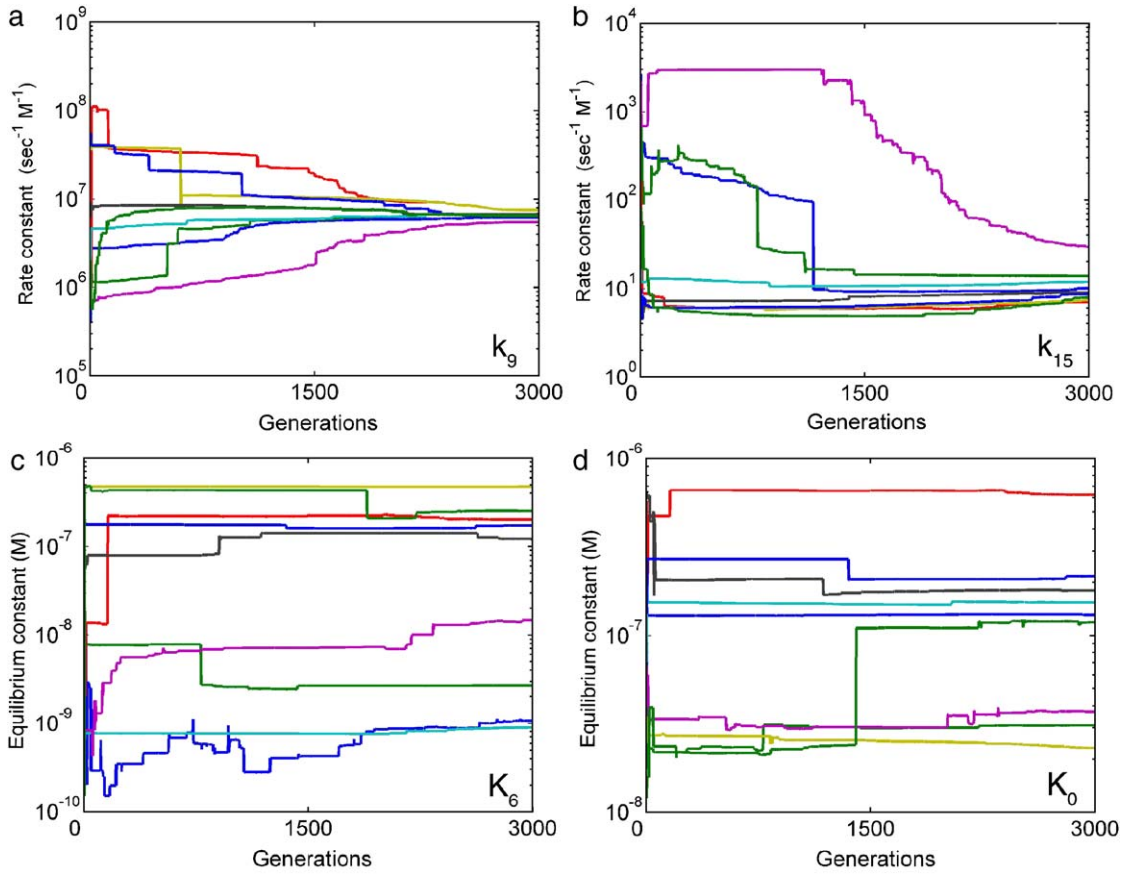

Fig. 2. The convergence of parameters during the Genetic Algorithm. The parameters are defined according to the reaction number in Scheme 1. Color represents different Runs. (a, b) The convergence of the rate constants corresponding to the final steps of the fusion process of k_9 (a) and k_{15} (b) during the reconstruction of the input signals. Please note that the converged values after 300 generations fall within a rather narrow range. (c, d) The variation with the number of generations of adjustable parameters that did not converge during the reconstruction K_6 (c) and K_0 (d). Please note the wide spread of those values.

ones obtained previously using other parameter optimization methods [27,36]. This suggests that the reconstruction of the basic kinetics of exocytosis is mainly determined by the relative amount of the two synaptotagmins' binding and the downstream steps of the 3 calcium binding and the fusion.

3.2. Increase of the complexity of the analyzed input data: constraint imposed by the calcium-dependent priming behavior

To increase the number of parameters that converged in the GA search, we used more experimental observations, which describe different features of the exocytotic process, as input signals. Accordingly, we added new penalty factors that describe these behaviors. Addition of more penalty factors to the fitness function increased the complexity of the GA search and forced the system to be more sensitive.

The first feature that was added to the system was the calcium-dependent priming behavior of exocytosis. Elevation of the pre-pulse [Ca^{2+}] has been shown to modulate the size of the exocytotic burst in chromaffin cells, a phenomenon that is known as calcium-dependent priming [29,37]. During this short pre-pulse phase of the exocytotic process, the Ca^{2+} ions (~200–300 nM) interact with the high affinity Ca^{2+} sites that regulate the maturation of the SNARE complex. This causes an increase in the number of primed vesicles and, as a result, following stimulation it will cause larger exocytosis during the exocytotic burst (measured up to 1 sec after the stimulation). There are three steps in the model where the low Ca^{2+} concentration affects the process: the activation of munc13 by calcium (reaction 0 in Scheme 1), the activation of SNARE into SNARE' by munc13′ (reaction 3) and the Ca^{2+} dependent conversion of SNARE' to SNARE* (reaction 4 in Scheme 1). To force the GA to retrace the experimental variation of the exocytotic burst on the pre-pulse [Ca^{2+}], we added penalty factors P_1, and P_2 (see Appendix A). In practice, the GA scored each phenotype also by its ability to reconstruct the input release signals (WT and SytIKO), and penalized it by its deviation from the observed dependence of the amplitude of the exocytotic burst on the pre-pulse Ca^{2+} concentration [29]. The function readily converged to fit both experimental inputs (Fig. 3).

Fig. 3 depicts the best-fit phenotype with the progression of the evolution. The upper left frame represents the reconstructed lines (gray) together with the experimental signals (WT and SytIKO, black), as calculated for the first generation. The other frames on the left represent the enhanced fitting as recorded after 10, 100 and 3000 generations, respectively. The right frames represent the calculated (gray) and the measured (black) exocytotic burst values versus pre pulse calcium, after 1, 10, 100 and 3000 generations. To enhance the speed of convergence, the rate constants, which were determined in the previous section, were allowed to vary within a narrower range (one order of magnitude). As these parameters were optimized for the WT and SytIKO experiments, we already achieved a relatively good fitting after one generation (Fig. 3, upper left), while the fitting to the new feature gradually improved over the generations (Fig. 3, right).

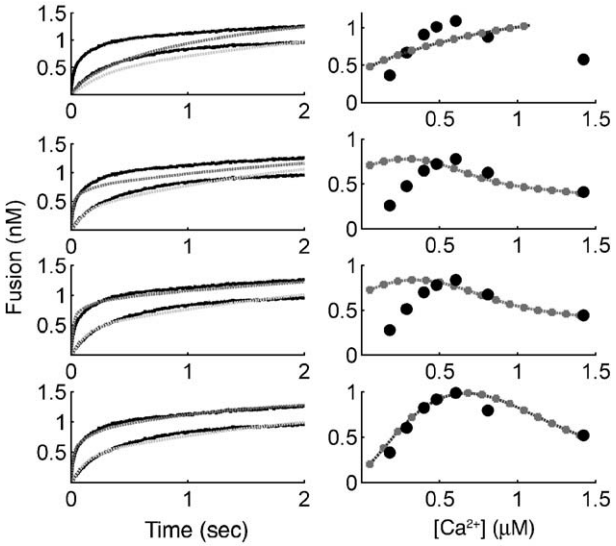

Fig. 3. The best-fit phenotypes with the progression of the GA evolution imposed by two constrains. The GA was set to reconstruct both the fusion dynamics for the WT and the SytIKO curves (left) and the relation between the exocytotic burst versus the pre-pulse Ca^{2+} (right). Each row represents the best fit phenotype after 1, 10, 100, and 3000 generations. Experimental data (black) GA signals (gray).

The analysis presented in Fig. 3 was repeated ~50 times and the distribution of the adjustable parameters revealed that some of the upstream parameters show better convergence. The improvement was obtained for the high calcium affinity binding steps (K_0, k_3, [Munc13-1]) and the rate (k_6, k_{11}) and equilibrium constants (K_6, K_{11}) of synaptotagmin binding to SNARE$^{\#}$. The highest degree of convergence was obtained for the equilibrium constant of the activation of Munc13 by calcium (step 0). It converged to a very narrow range between 300 and 600 nM (Table 2). On the other hand, the rate constant for the activation of Munc13 by calcium (k_0) did not converge. Apparently, within the kinetic requirement of the system, the level of activated Munc13 and not the rate of calcium binding to Munc13, determines the calcium-dependent priming behavior. This is a reasonable conclusion, since calcium ions are not a limiting factor under these conditions; rather, the calcium concentration itself controls the binding. Interestingly, this K_d is similar to the calcium range that controls the priming process as seen from the observed dependence of the amplitude of the exocytotic burst on the pre-pulse Ca^{2+} concentration [29]. In addition, the convergence of most upstream parameters in these experiments supports our previous suggestion that priming is a multiple step process [8].

3.3. Analysis of the exocytotic process using four optimizing features

To enhance the convergence of the adjustable parameters, we stiffen the fitting problem by adding another experimental protocol together with the appropriate new penalty factors for the GA search. The experimental feature that describes the dynamics of the recovery of the releasable pool after exhaustive stimulation was added to the GA search as a new input signal.

Experimentally, Voets and coworkers [28] stimulated cells by four successive depolarizations (100 ms each) that specifically depleted the readily releasable pool (RRP), and then allowed the cell to recover for a variable time frame (0.5–80 s) before being challenged by a high Ca^{2+} pulse (flash). The initial recovery of the RRP was mirrored by a gradual decrease in the slowly releasable pool (SRP). After a recovery time of about 30 s, the build-up of the RRP was not associated with a decrease in the SRP size and both "pools" increased linearly with time. Based on this observation, Voets and coworkers [28] suggested that the recovery of the RRP occurs at the expense of the SRP. In a previous publication [8], we had demonstrated that the RRP and SRP "pools" can be equated with the RC-I and RC-II reservoirs, which are in equilibrium with a common species $SNARE^{\#}$. Accordingly, we could retrace these results [28] through the model. The GA was modified to include the appropriate penalty factor for P3, P_4 and P_5 (see Appendix A), which penalizes the fitness function value by its ability to reconstruct the experimental observations [28].

Once the four features were used for optimization (see Fig. 4), the convergence was enhanced, and the fitness function reached its plateau already after ~50 generations, while the analysis as in Fig. 3 needed ~500 generations to gain their final level. Addition of this constraint to the GA led to the fact that the rate and equilibrium constants of the steps that interconnect RCI and RCII (reactions 6, 11) show a higher degree of convergence; specifically, the on rate of the binding of synaptotagmin I (k_6). Thus the main steps that control the shift from RCI to RCII are the rate constants of the synaptotagmin's binding. In addition, the use of all four constraints improved the convergence of the other rate constants, including those that did not converge in the GA runs in which we used only part of the constraints (Fig. 1 and Fig. 3). The range of the variation for each adjustable parameter is summed up in Table 2, column 4. The best 10 solutions were selected and the mean values plus standard deviations for each adjustable parameter were calculated (see Table 2, columns 5 and 6).

The robustness [38] of the model demands that a random combination of values falling within the limits of the range of variance (column 4 in Table 2) will generate curves that retain the general features of the dynamics. This was tested by generating 200 combinations of parameters that were randomly selected from the range given in column 4 in Table 2, and the corresponding shape of the reconstructed signals was checked. In all cases, the release dynamics exhibit well resolved 'fast' and 'slow' release phases, with a clear separation between the 'WT' and the 'SytIKO' mutant. These random combinations also yielded a bell shape dependence of exocytosis on the pre-pulse Ca^{2+}, and typical recovery dynamics (not shown). Thus, the multi-dimensional parameter space within the range illustrated in Table 1 column 4 defined the domain where the solution is stable.

Further analysis of the variables was carried out as in Moscovitch et al. [16]. The Normal Probability plot analysis, as implemented by the Matlab QQplot function, relates the individual value with respect to the mean value calculated for the same variable. When the quantile analysis generates a linear function, it implies that values are members of a single, normal population. Thus, for each of the adjustable parameters, there is a single value where the fitness function will be minimal.

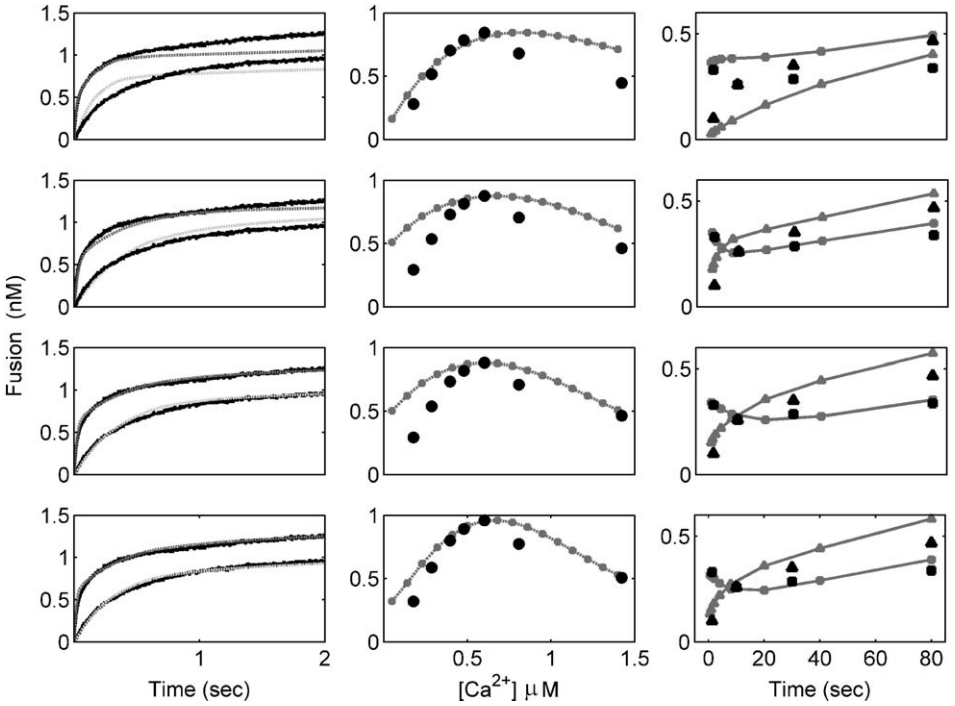

Fig. 4. The evolution of the reconstruction as a function of the number of generations under all four constrains. The simulations retrace the fusion dynamics for the WT and the SytIKO mutants (left curves), the values of the exocytotic burst versus the pre-pulse Ca^2 (middle curves) and the recovery after depolarization pulses (right curves). Each row represents the best fit phenotype after 1, 10, 30, and 3000 generations. RRP size (triangles) SRP size (squares). Experimental data (black) GA signals (gray).

Moreover, the normal variance between the values attained for each parameter implies that the convergence followed random trajectories in the multi-dimensional parameter space. The quantile analysis had been carried out for all variables, and in all cases a linear relationship was observed (Fig. 5). We can therefore suggest that the combination of the mean values represents the global minimum of the fitness function in the multi-dimensional parameter space.

3.4. Testing of the model

Mathematical models can be tested by the requirement to reproduce features for which the model was not optimized. In our previous publication [8], we demonstrated that the parameters appearing in the present study were able to reproduce the dependence of the rate of release on [Ca^{2+}] and to predict the change in the amplitude caused by overexpression of munc 13. In the present study we also investigated whether the parameters selected by the GA can reproduce the delay time of the release reaction.

Kinetic measurements of the earliest event, following flash photolysis of caged calcium, revealed a distinct delay (lag phase) in the fusion kinetics. The length of the lag phase varies from almost 100 ms at low Ca^{+2} concentration following the flash down to a few ms at high calcium concentrations [29,36]. We tested the model both qualitatively and quantitatively with the GA parameters. The qualitative evaluation was carried out by examining the early events that precede fusion in order to test whether the parameters selected by the GA can reproduce the experimental delay. The quantitative test was a comparison between the length of the calculated and the measured lag times as they vary with [Ca^{2+}] following the calcium pulse (flash) (Fig. 6).

Fig. 6a reproduced the initial phase of fusion in the model. We plotted the experimental signal together with the dynamics of the intermediate protein complexes located between the RC-I complex and the final fused state. The dynamics of the slow fusing complex RC-II were omitted, as their fusion is 10 times slower and makes no contribution to the lag time. As seen in Fig. 6a, the calculated and the measured curves overlap, even though the events during the initial time frame contributed less than 0.1% to the value of the fitness function. Moreover, the model also provides an explanation for the lag time. This delay corresponds to the 3 sequential calcium binding steps, until the final RC-I-3Ca^{+2} are formed.

While Fig. 6a demonstrates that the model can reproduce the lag time, Fig. 6b correlates between the length of the lag time and the Ca^{2+} concentration that triggered the fusion reaction for the experimental (Fig. 6b, crosses) [36] and the simulation (Fig. 6b, circle) data. The lag time in the simulation was defined as the time frame needed for the reconstructed curve to reach the level of 1% from its maximal value. The correlation between the calculated and measured values is self-evident. Apparently, the parameters selected for reproducing the various features of the fusion are suitable for reconstruction of features that were not used for the optimization of the GA and minimization of the fitness function's value.

3.5. The versatility of the model

The present state of the model is compatible with the current data regarding the interactions of 7 synaptic proteins, forming the active SNARE complexes and their activation by free calcium ions. As the exocytotic process is probably mediated by more proteins, it is essential to investigate whether the model is

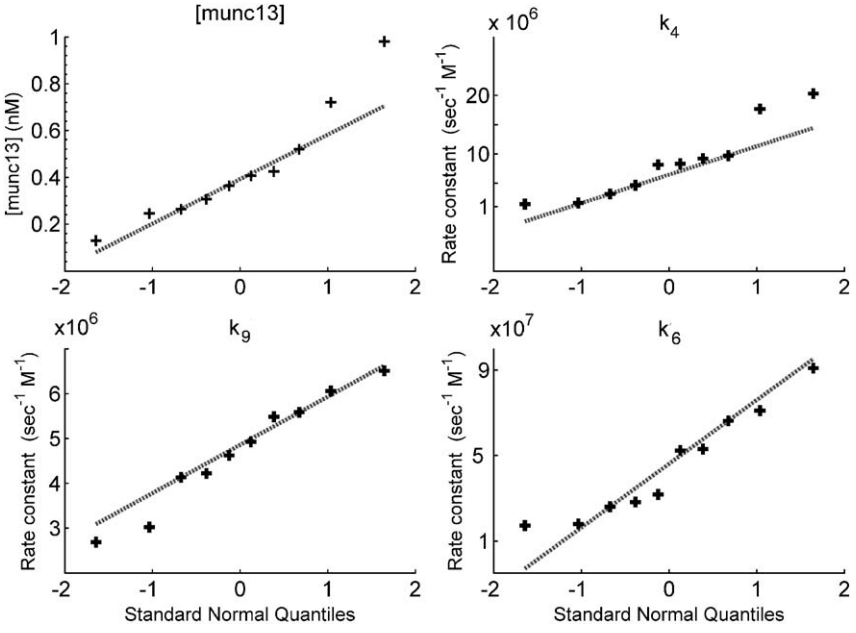

Fig. 5. Quantile analysis of the best-fitted solutions. The Genetic Algorithm generated 34 independent solutions for the system detailed in Fig. 4. For the best 10 solutions, the mean and standard deviations were calculated by the QQPLOT function of Matlab and the distributions of the values with respect to the mean value were analyzed. Each frame in the figure relates to the measured value (ordinate) with the standard normal quantile drawn on the abscissa. For brevity, the results are presented for only four adjustable parameters.

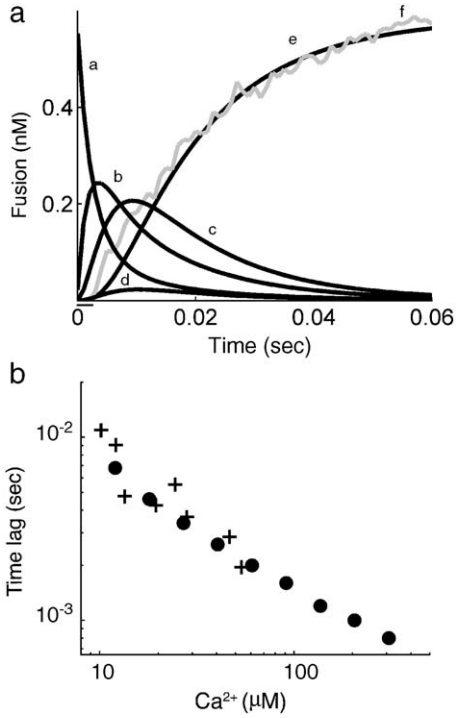

Fig. 6. Tracing of the earliest phase of the fusion dynamics. (a) Superposition of the fusion dynamics (curve f, gray) and the reconstructed dynamics (curve e, black) during the first 60 ms after the calcium pulse. Following the high Ca^{2+} pulse, at $t=0$, the RC-I state of the vesicles is rapidly depleted (curve a) with subsequent accumulation of the first Ca^{2+} complex RC-I-1Ca (curve b). This complex is converted with a delay into the higher Ca^{2+} complexes RC-I-2Ca (curve c); RC-I-3Ca (curve d) and the fusion products (curve e). These transitions create the short delay (bar). (b) The correlation between the length of the lag time and the Ca^{+2} concentration of the pulse. (Pluses) The experimental results as reported by Voets et al. [36]. (circles) The length of the lag time calculated from the simulation corresponding to the experimental conditions of Voets et al. [36]. The lag time was defined as the time frame, after the Ca^{+2} pulse, needed for the amplitude to reach 1% of its maximal value.

versatile and can be expanded when new kinetic information is revealed. To evaluate the versatility of the model, we carried out two set of calculations; in one, we deliberately removed a well-established component of the system, and in the other, we increased the number of Ca^{2+} ions needed for initiation of the final fusion event.

As a test for the ability of the model to incorporate unknown reaction steps, we deliberately mutilated the sequence of the reactions by removing a well-established step. Our expectations from a versatile model is to reconstruct the observation with the same rate constants, except for the 'bridge' step, in which the parameters will vary in order to compensate for the missing event.

The omitted reaction was the binding of complexin to the SNARE* complex, generating a pathway pretending that the $SNARE^{\#}$ complex is a direct product of the activation of SNARE' by the Ca^{2+} ions (reaction 4 in Scheme 1). The reaction sequence without the involvement of complexin as a reactant was converted into a set of differential rate equations, and subjected to kinetic analysis that consisted of the four optimization features described above. The search yielded a new solution that reconstructed the experimental results with the same level of accuracy of the standard model where the adjustable parameters were essentially the same except for the step where the component had been removed. The omission of complexin from the reaction sequence was fully ameliorated by a 50-fold increase of the Ca^{2+} affinity of reaction 4, reducing K_{eq} from 560 nM to an extremely low value of 10 nM. The above calculation, where an established component of the reaction system is removed, demonstrates that the model is sufficiently robust to suffer a shortening of the reaction sequence, and still reconstructs the experimental observation. In practice, we expect a reverse situation where future experimental study will reveal the presence of new proteins associated with the exocytotic pathway, either within the section discussed in the present study or in earlier events.

The versatility of the model was also evaluated by modulating the number of Ca^{2+} binding sites needed to initiate the fusion. It is generally agreed that the rate of release is an exponential function of the Ca^{2+} concentration ($[Ca^{2+}]^{m}$; $m \geq 3$). In chromaffin cells, the apparent value of the exponent is m ~3, yet in other systems (such as the Calyx of Held synapse [39] or under conditions of non-homogenous intra-cellular Ca^{2+} distributions [40], the value of m was found to vary ($3 \leq m \leq 5$), depending on the precise experimental conditions. The present model had used $m=3$ to comply with the experimental results. However, on testing the model, suitable simulations could be obtained with values of $m \geq 3$ with proper compensation through the magnitude of the rate constant (data not shown). Thus, when applying the model to other cells, the cooperativity can be modulated without loss of the applicability of the model.

It is of interest to point out that as most of the rate constants values described in this model are slower than the upper estimation for diffusion-controlled reactions, this observation implies that the actual reaction steps consist of more than a single step or process. These hidden steps or processes can either be a conformational change of the proteins, a reaction with another (still unidentified) protein(s) or even oligomerization of proteins, such as the oligomerization of the SNARE complexes or of synaptotagmin. These oligomerizations can either accelerate the formation of SNARE# or change the calcium cooperativity [41–43]. At present, we cannot ascertain those events that slow the overall rate, yet we can assume that each of the reaction steps is a sequence of molecular events and only their overall combination of time constants is expressed by the rate constant, as was determined by the analysis. In accordance with this concept, the present reaction scheme should be considered as expandable and suitable to accommodate a more refined pattern of events.

We presently recognize quite a few neuro-degenerative diseases, where the exocytotic apparatus appears to be impaired. Once the model had been accepted as a proper representation of the exocytosis, kinetic analysis of standard parameters of the mechanism, as those discussed in the present publication, may be used in order to define the reaction steps where the values of the adjustable parameters had markedly changed. This suggests that the malfunction may be associated with the very same step. Thus, we suggest that accepting the system described in the present study as a standard representation of the exocytotic

process may be evolved into a diagnostic tool, revealing the sites where the sequence of events is fundamentally impaired.

4. Concluding remarks

In the present study, we investigated a complex cellular process using the formalism of classical chemical kinetics. To cope with the huge number of possible solutions of the system, and to eliminate human influence, we employed the GA for a systematic search in a multi-dimensional parameter space. To our surprise, the search yielded a consistent solution, which testified to the robustness of the model. A large number of independent searches converged into a single minimum for the fitness function in the multi-dimensional parameter space. A gradual increase of the complexity of the analyzed input data brought specific parameters to corresponding convergence, and allowed correlation between the experimental data and the reactions that they represent. The present study indicated that the GA is an effective tool for intensive search into a multi-dimensional parameter space, which is capable of convergence into the unique solution of complex biological systems.

Acknowledgements

We thank Dr. Thomas Voets for providing the raw data for various experiments. This research was supported by grants from the Yeshaya Horowitz Association through the Center for Complexity science (to U.A., M.G., G.F., and M.A), the Minerva Junior Research Group (to U.A.); The Israeli Science Foundation (472/01-2). The American Israel Binational Science Foundation (2002129) (to M.G.); and the Constantiner Foundation (to M.A.).

Appendix A

The value of the fitness function (Eq. (1)) is the product of the difference between the calculated and measured values as in Eq. (2), and the various penalty factors defined by Eq. (3a), and (3b). The terms $r_{(i)}$ are defined by Eqs. (4a)–(4e) and the Q values are given in Eq. (5a) and (5b).

$$Ft(t) = ft(t) \times \prod_{1}^{6} P(i) \tag{1}$$

$$ft(t) = \sum_{t} \left(\frac{(\text{calculated WT}_t - \text{signal WT}_t)}{\text{signal WT}} \right)^2 + \left(\frac{(\text{calculated KO}_t - \text{signal KO}_t)}{\text{signal WT}} \right)^2 \tag{2}$$

$$\{P_i | i = 1..5\} = \begin{cases} 1 & R_i = r_i \\ |r_i - R_i|^2 \times Q_i + 1 & R_i \neq r_i \end{cases} \tag{3a}$$

$$R_1 = 2; R_2 = 2; R_3 = 0.33; R_4 = 1; R_5 = 1.5;$$

$$P_6(t) = \begin{cases} 2 & t < 1\text{s} \\ 1 & t > 1\text{s} \end{cases} \tag{3b}$$

$$r(1) = \frac{\text{calculated value}(\text{Ca} = 540\ \text{nM})}{\text{calculated value} = 180\ \text{nM}} \tag{4a}$$

$$r(2) = \frac{\text{calculated value}(\text{Ca} = 540\ \text{nM})}{\text{calculated value} = 1620\ \text{nM}} \tag{4b}$$

$$r(3) = \frac{\text{calculated RCI}(t = 0\ \text{s})}{\text{calculated RCII}(t = 0\ \text{s})} \tag{4c}$$

$$r(4) = \frac{\text{calculated RCI}(t = 10\ \text{s})}{\text{calculated RCII}(t = 10\ \text{s})} \tag{4d}$$

$$r(5) = \frac{\text{calculated RCI}(t = 100\ \text{s})}{\text{calculated RCII}(t = 100\ \text{s})} \tag{4e}$$

$$\{Q_i | i = 1,\ 2\} = 0.9 \tag{5a}$$

$$\{Q_i | i = 3..5\} = 0.2 \tag{5b}$$

The $r(1, 2)$ are the ratios of the amplitude, calculated 1 second after the high Ca^{+2} pulse, at given pre-pulse [Ca^{+2}] concentrations (as marked in the Eqs. (4a) (4b)).

$r(3, 4, 5)$ are the ratios between the amplitudes assigned to PathI and PathII at the given time values (marked in the Eqs. (4c) (4d) (4e)) during the recovery of the system after exhaustive depolarization.

$R(1–5)$ (in Eq. (3a)) are the experimental values of $r(1–5)$ as determined from the measurements of Voets et al. [28,29].

The $Q(1, 2)$, (in Eq. (5a)) are adjustable parameters operating on the penalty factors which allow us to balance the correction factors in order to gain the best results.

References

[1] J.T. Littleton, H.J. Bellen, Presynaptic proteins involved in exocytosis in *Drosophila melanogaster*: a genetic analysis, Invertebr. Neurosci. 1 (1995) 3–13.
[2] R. Fernandez-Chacon, T.C. Sudhof, Genetics of synaptic vesicle function: toward the complete functional anatomy of an organelle, Annu. Rev. Physiol. 61 (1999) 753–776.
[3] R. Jahn, T.C. Sudhof, Membrane fusion and exocytosis, Annu. Rev. Biochem. 68 (1999) 863–911.
[4] T.C. Sudhof, The synaptic vesicle cycle revisited, Neuron 28 (2000) 317–320.
[5] J. Rettig, E. Neher, Emerging roles of presynaptic proteins in Ca++ triggered exocytosis, Science 298 (2002) 781–785.
[6] J. Richmond, K. Broadie, The synaptic vesicle cycle: exocytosis and endocytosis in *Drosophila* and *C. elegans*, Curr. Opin. Neurobiol. 12 (2002) 499–507.

[7] C. Rosenmund, J. Rettig, N. Brose, Molecular mechanisms of active zone function, Curr. Opin. Neurobiol. 13 (2003) 509–519.
[8] A. Mezer, M. Gutman, E. Nachliel, U. Ashery, A new platform to study the molecular mechanisms of exocytosis, J. Neurosci. 24 (2004) 8838–8846.
[9] J.H. Holland, Robust algorithms for adaptation set in a general formal framework, Proceedings of the 1970 IEEE symposium on adaptive processes (9th) decision and control, 1970, 5.
[10] R. Leardi, Genetic Algorithm in chemometrics and chemistry: a review, J. Chemom. 15 (2001) 559–569.
[11] B. Filipic, I. Zun, M. Perpar, Skill-based interpretation of noisy probe signals enhanced with a genetic algorithm, Int. J. Human-Comput. Stud. 53 (2000) 517–535.
[12] C. Hongqing, Y. Jingxian, K. Lishan, C. Yuping, C. Yongyan, The kinetic evolutionary modeling of complex systems of chemical reactions, Comput. Chem. 23 (1999) 143–151.
[13] C. Houck, J. Joines, M.A. Kay, Genetic algorithm for function optimization: A Matlab implementation NCSU-IE TR (1995) 95–09.
[14] D.B. Terry, M. Messina, Heuristic search algorithms for the determination of rate constants and reaction mechanisms from limited concentration data, J. Chem. Inf. Comput. Sci. 38 (1998) 1232–1238.
[15] C. Viappiani, G. Bonetti, M. Carelli, F. Ferrati, A. Sternieni, Study of proton transfer processes in solutions using the laser induced pH jump: a new experimental setup and an improved data analysis based on genetic algoriths, Rev. Sci. Instrum. 69 (1998) 270–276.
[16] D. Moscovitch, O. Noivirt, A. Mezer, E. Nachliel, T. Mark, M. Gutman, G. Fibich, Determination of a unique solution to parallel proton transfer reactions using the genetic algorithm, Biophys. J. 87 (2004) 47–57.
[17] D. Fasshauer, M. Margittai, A transient interaction of SNAP-25 and syntaxin nucleates SNARE assembly, J. Biol. Chem. 297 (2004) 7613–7621.
[18] T. Lang, D. Bruns, D. Wenzel, D. Riedel, P. Holroyd, C. Thiele, R. Jahn, SNAREs are concentrated in cholesterol-dependent clusters that define docking and fusion sites for exocytosis, EMBO J. 20 (2001) 2202–2213.
[19] C. Rickman, F.A. Meunier, T. Binz, B. Davletov, High affinity interaction of syntaxin and SNAP-25 on the plasma membrane is abolished by botulinum toxin E, J. Biol. Chem. 279 (2004) 644–651.
[20] R.B. Sutton, D. Fasshauer, R. Jahn, A.T. Brunger, Crystal structure of a SNARE complex involved in synaptic exocytosis at 2.4 A resolution, Nature 395 (1998) 347–353.
[21] T. Weber, B.V. Zemelman, J.A. McNew, B. Westermann, M. Gmachl, F. Parlati, T.H. Sollner, J.E. Rothman, SNAREpins: minimal machinery for membrane fusion, Cell 92 (1998) 759–772.
[22] K.E. Marz, P.I. Hanson, Sealed with a twist: complexin and the synaptic SNARE complex, Trends Neurosci. 25 (2002) 381–383.
[23] X. Chen, D.R. Tomchick, E. Kovrigin, D. Arac, M. Machius, T.C. Sudhof, J. Rizo, Three-dimensional structure of the complexin/SNARE complex, Neuron 33 (2002) 397–409.
[24] S. Pabst, M. Margittai, D. Vainius, R. Langen, R. Jahn, D. Fasshauer, Rapid and selective binding to the synaptic SNARE complex suggests a modulatory role of complexins in neuroexocytosis, J. Biol. Chem. 277 (2002) 7838–7848.
[25] K. Reim, M. Mansour, F. Varoqueaux, H.T. McMahon, T.C. Sudhof, N. Brose, C. Rosenmund, Complexins regulate a late step in Ca2+-dependent neurotransmitter release, Cell 104 (2001) 71–81.
[26] J.B. Sorensen, R. Fernandez-Chacon, T.C. Sudhof, E. Neher, Examining synaptotagmin 1 function in dense core vesicle exocytosis under direct control of Ca2+, J. Gen. Physiol. 122 (2003) 265–276.
[27] J.B. Sorensen, U. Matti, S.H. Wei, R.B. Nehring, T. Voets, U. Ashery, T. Binz, E. Neher, J. Rettig, The SNARE protein SNAP-25 is linked to fast calcium triggering of exocytosis, Proc. Natl. Acad. Sci. U. S. A. 99 (2002) 1627–1632.
[28] T. Voets, E. Neher, T. Moser, Mechanisms underlying phasic and sustained secretion in chromaffin cells from mouse adrenal slices, Neuron 23 (1999) 607–615.
[29] T. Voets, Dissection of three Ca2+-dependent steps leading to secretion in chromaffin cells from mouse adrenal slices, Neuron 28 (2000) 537–545.
[30] X.Z. Xu, P.D. Wes, H. Chen, H.S. Li, M. Yu, S. Morgan, Y. Liu, C. Montell, Retinal targets for calmodulin include proteins implicated in synaptic transmission, J. Biol. Chem. 273 (1998) 31297–31307.
[31] J.S. Rhee, A. Betz, S. Pyott, K. Reim, F. Varoqueaux, I. Augustin, D. Hesse, T.C. Sudhof, M. Takahashi, C. Rosenmund, N. Brose, Beta phorbol ester- and diacylglycerol-induced augmentation of transmitter release is mediated by Munc13s and not by PKCs, Cell 108 (2002) 121–133.
[32] N. Brose, K. Hofmann, Y. Hata, T.C. Sudhof, Mammalian homologues of *Caenorhabditis elegans* unc-13 gene define novel family of C2-domain proteins, J. Biol. Chem. 270 (1995) 25273–25280.
[33] U. Ashery, F. Varoqueaux, T. Voets, A. Betz, P. Thakur, H. Koch, E. Neher, N. Brose, J. Rettig, Munc13-1 acts as a priming factor for large dense-core vesicles in bovine chromaffin cells, EMBO J. 19 (2000) 3586–3596.
[34] T. Xu, T. Binz, H. Niemann, E. Neher, Multiple kinetic components of exocytosis distinguished by neurotoxin sensitivity, Nat. Neurosci. 1 (1998) 192–200.
[35] M. Gutman, E. Nachliel, Time resolved dynamics of proton transfer in proteinous systems, Annu. Rev. Phys. Chem. 48 (1997) 329–356.
[36] T. Voets, T. Moser, P.E. Lund, R.H. Chow, M. Geppert, T.C. Sudhof, E. Neher, Intracellular calcium dependence of large dense-core vesicle exocytosis in the absence of synaptotagmin I, Proc. Natl. Acad. Sci. U. S. A. 98 (2001) 11680–11685.
[37] L. von Ruden, E. Neher, A Ca-dependent early step in the release of catecholamines from adrenal chromaffin cells, Science 262 (1993) 1061–1065.
[38] N. Barkai, S. Leibler, Robustness in simple biochemical networks, Nature 387 (1997) 317–913.
[39] R. Schneggenburger, E. Neher, Intracellular calcium dependence of transmitter release rates at a fast central synapse, Nature 406 (2000) 889–893.
[40] V. Shahrezaei, K.R. Delaney, Brevity of the Ca2+ microdomain and active zone geometry prevent Ca2+-sensor saturation for neurotransmitter release, J. Neurophysiol. 94 (2005) 1912–1919.
[41] Y. Hua, R.H. Scheller, Three SNARE complexes cooperate to mediate membrane fusion, Proc. Natl. Acad. Sci. U. S. A. 98 (2001) 8065–8070.
[42] X. Han, C.T. Wang, J. Bai, E.R. Chapman, M.B. Jackson, Transmembrane segments of syntaxin line the fusion pore of Ca2+-triggered exocytosis, Science 304 (2004) 289–292.
[43] B.A. Stewart, M. Mohtashami, W.S. Trimble, G.L. Boulianne, SNARE proteins contribute to calcium cooperativity of synaptic transmission, Proc. Natl. Acad. Sci. U. S. A. 97 (2000) 13955–13960.
[44] M. Margittai, J. Widengren, E. Schweinberger, G.F. Schroder, S. Felekyan, E. Haustein, M. Konig, D. Fasshauer, H. Grubmuller, R. Jahn, C.A. Seidel, Single-molecule fluorescence resonance energy transfer reveals a dynamic equilibrium between closed and open conformations of syntaxin 1, Proc. Natl. Acad. Sci. U. S. A. 100 (2003) 15516–15521.
[45] K. Weninger, M.E. Bowen, S. Chu, A.T. Brunger, Single-molecule studies of SNARE complex assembly reveal parallel and antiparallel configurations, Proc. Natl. Acad. Sci. U. S. A. 100 (25) (2003 (Dec 9)) 14800–14805.
[46] E.M. Graham, J.R. Barclay, R.D. Burgoyne, Syntaxin/munc18 interactions in the late events during vesicle fusion and release in exocytosis, J. Biol. Chem. 279 (2004) 32751–32760.